Science
AAAS

Climate Sensitivity Estimated from Temperature Reconstructions of the Last Glacial Maximum

Andreas Schmittner, *et al.*

Science **334**, 1385 (2011);
DOI: 10.1126/science.1203513

This copy is for your personal, non-commercial use only.

If you wish to distribute this article to others, you can order high-quality copies for your colleagues, clients, or customers by clicking here.

Permission to republish or repurpose articles or portions of articles can be obtained by following the guidelines here.

The following resources related to this article are available online at www.sciencemag.org (this infomation is current as of December 12, 2011):

Updated information and services, including high-resolution figures, can be found in the online version of this article at:
http://www.sciencemag.org/content/334/6061/1385.full.html

Supporting Online Material can be found at:
http://www.sciencemag.org/content/suppl/2011/11/23/science.1203513.DC1.html

A list of selected additional articles on the Science Web sites **related to this article** can be found at:
http://www.sciencemag.org/content/334/6061/1385.full.html#related

This article **cites 98 articles**, 12 of which can be accessed free:
http://www.sciencemag.org/content/334/6061/1385.full.html#ref-list-1

This article has been **cited by** 1 articles hosted by HighWire Press; see:
http://www.sciencemag.org/content/334/6061/1385.full.html#related-urls

This article appears in the following **subject collections:**
Atmospheric Science
http://www.sciencemag.org/cgi/collection/atmos

Downloaded from www.sciencemag.org on December 12, 2011

Science (print ISSN 0036-8075; online ISSN 1095-9203) is published weekly, except the last week in December, by the American Association for the Advancement of Science, 1200 New York Avenue NW, Washington, DC 20005. Copyright 2011 by the American Association for the Advancement of Science; all rights reserved. The title *Science* is a registered trademark of AAAS.

The OER design principle shown in Fig. 2 was applied to obtain a highly active OER catalyst, BSCF, which was best known for its high performance as a cathode in solid oxide fuel cells (*27*) and oxygen permeation membranes. Because the surface Co cations of BSCF are in the intermediate spin state (*28*, *29*), the electronic configuration of Co cations (estimated oxidation state of ~2.8; table S3) in BSCF can be assigned as $t_{2g}^{5}e_{g}^{\sim 1.2}$. We found that BSCF (fig. S3) had the highest OER activity among all oxides studied as predicted by the e_g activity descriptor (Fig. 2). To ensure that the observed oxidation current was from oxygen evolution, we used a rotating Pt ring electrode held at the ORR potential of 0.4 V versus RHE to detect O_2 gas generated at the catalyst by electrochemical reduction (Fig. 3A). The reduction current detected on the ring electrode suggested that the oxidation current from BSCF could be accounted for fully by the OER. The measured intrinsic OER activity of BSCF was higher than that of IrO_2 nanoparticles (average diameter ~6 nm) (Fig. 3B) by at least an order of magnitude when considering a conservative experimental uncertainty in the intrinsic OER activity of approximately an order of magnitude (*24*). The exceptional OER activity of BSCF was further confirmed by galvanostatic measurements, which manifested no degradation in the OER activity (fig. S4). Once the sizes of BSCF particles were reduced to submicrometer range via ball-milling, the mass activity of ball-milled BSCF (BM-BSCF) was found to compare favorably with IrO_2, and the overpotential of BM-BSCF was shown to be nearly identical to that of IrO_2 at a catalytic activity normalized to the catalyst's mass (i.e., mass activity) of 10 A g_{ox}^{-1} (Fig. 3C). Developing nanostructured BSCF could further improve its mass activity and thus yield highly efficient OER electrodes.

Our study suggests the importance of developing a transition metal oxide having a surface cation e_g occupancy close to unity and high B-site oxygen covalency for enhancing the OER catalytic activity. This approach is a promising strategy to create bifunctional oxide catalysts and electrodes for the development of efficient, rechargeable metal-air batteries, regenerative fuel cells, and other rechargeable air-based energy storage devices.

References and Notes

1. H. B. Gray, *Nat. Chem.* **1**, 7 (2009).
2. N. S. Lewis, D. G. Nocera, *Proc. Natl. Acad. Sci. U.S.A.* **103**, 15729 (2006).
3. M. W. Kanan, D. G. Nocera, *Science* **321**, 1072 (2008).
4. Y. C. Lu *et al.*, *J. Am. Chem. Soc.* **132**, 12170 (2010).
5. M. Armand, J. M. Tarascon, *Nature* **451**, 652 (2008).
6. M. T. M. Koper, *J. Electroanal. Chem.* **660**, 254 (2011).
7. J. Rossmeisl, Z. W. Qu, H. Zhu, G. J. Kroes, J. K. Norskov, *J. Electroanal. Chem.* **607**, 83 (2007).
8. H. A. Gasteiger, N. M. Marković, *Science* **324**, 48 (2009).
9. V. R. Stamenkovic *et al.*, *Science* **315**, 493 (2007).
10. H. A. Gasteiger, S. S. Kocha, B. Sompalli, F. T. Wagner, *Appl. Catal. B* **56**, 9 (2005).
11. C. R. Davidson, G. Kissel, S. Srinivasan, *J. Electroanal. Chem.* **132**, 129 (1982).
12. J. O. Bockris, T. Otagawa, *J. Electrochem. Soc.* **131**, 290 (1984).
13. S. Trasatti, *J. Electroanal. Chem.* **111**, 125 (1980).
14. I. C. Man *et al.*, *ChemCatChem* **3**, 1159 (2011).
15. B. Hammer, J. K. Nørskov, *Adv. Catal.* **45**, 71 (2000).
16. C. J. Ballhausen, H. B. Gray, *Inorg. Chem.* **1**, 111 (1962).
17. T. A. Betley, Q. Wu, T. Van Voorhis, D. G. Nocera, *Inorg. Chem.* **47**, 1849 (2008).
18. J. Suntivich, H. A. Gasteiger, N. Yabuuchi, Y. Shao-horn, *J. Electrochem. Soc.* **157**, B1263 (2010).
19. Y. Matsumoto, J. Kurimoto, E. Sato, *J. Electroanal. Chem.* **102**, 77 (1979).
20. Y. Matsumoto, H. Manabe, E. Sato, *J. Electrochem. Soc.* **127**, 811 (1980).
21. Y. Matsumoto, E. Sato, *Electrochim. Acta* **24**, 421 (1979).
22. A. Wattiaux, J. C. Grenier, M. Pouchard, P. Hagenmuller, *J. Electrochem. Soc.* **134**, 1714 (1987).
23. T. J. Schmidt *et al.*, *J. Electrochem. Soc.* **145**, 2354 (1998).
24. See supporting material on *Science* Online.
25. J. Q. Yan, J. S. Zhou, J. B. Goodenough, *Phys. Rev. B* **70**, 014402 (2004).
26. J. Suntivich *et al.*, *Nat. Chem.* **3**, 546 (2011).
27. Z. P. Shao, S. M. Haile, *Nature* **431**, 170 (2004).
28. A. S. Harvey *et al.*, *Phys. Chem. Chem. Phys.* **11**, 3090 (2009).
29. A. S. Harvey *et al.*, *J. Phys. Condens. Matter* **21**, 015801 (2009).

Acknowledgments: Supported by a Chesonis Foundation Fellowship (J.S.), a Natural Sciences and Engineering Research Council of Canada postgraduate scholarship (K.J.M.), the Robert A. Welch Foundation (J.B.G.), and the U.S. Department of Energy Hydrogen Initiative program under award DE-FG02-05ER15728. The research made use of the Shared Experimental Facilities supported by the MRSEC Program of the National Science Foundation under award DMR 08-019762. We acknowledge collaboration with H. Nakanishi (Toyota Motor Corporation). We thank Y. Lee, N. Yabuuchi, and L. Wang (oxide synthesis), D. G. Kwabi and A. N. Mansour (x-ray absorption), C. K. Brozek and M. Dinca (surface area measurements), and Exponent (thermogravimetry). The National Synchrotron Light Source is supported by the U.S. Department of Energy, Division of Material Sciences and Division of Chemical Sciences, under contract DE-AC02-98CH10886. Beamline X11 is supported by the Office of Naval Research and contributions from Participating Research Team members. A patent related to this invention has been filed.

Supporting Online Material

www.sciencemag.org/cgi/content/full/science.1212858/DC1
Materials and Methods
Figs. S1 to S7
Tables S1 to S5
Schemes S1 and S2
References (*30*–*47*)

18 August 2011; accepted 11 October 2011
Published online 27 October 2011;
10.1126/science.1212858

Climate Sensitivity Estimated from Temperature Reconstructions of the Last Glacial Maximum

Andreas Schmittner,[1]* Nathan M. Urban,[2] Jeremy D. Shakun,[3] Natalie M. Mahowald,[4] Peter U. Clark,[5] Patrick J. Bartlein,[6] Alan C. Mix,[1] Antoni Rosell-Melé[7]

Assessing the impact of future anthropogenic carbon emissions is currently impeded by uncertainties in our knowledge of equilibrium climate sensitivity to atmospheric carbon dioxide doubling. Previous studies suggest 3 kelvin (K) as the best estimate, 2 to 4.5 K as the 66% probability range, and nonzero probabilities for much higher values, the latter implying a small chance of high-impact climate changes that would be difficult to avoid. Here, combining extensive sea and land surface temperature reconstructions from the Last Glacial Maximum with climate model simulations, we estimate a lower median (2.3 K) and reduced uncertainty (1.7 to 2.6 K as the 66% probability range, which can be widened using alternate assumptions or data subsets). Assuming that paleoclimatic constraints apply to the future, as predicted by our model, these results imply a lower probability of imminent extreme climatic change than previously thought.

Climate sensitivity is the change in global mean near-surface air temperature ΔSAT caused by an arbitrary perturbation ΔF (radiative forcing) of Earth's radiative balance at the top of the atmosphere with respect to a given reference state. The equilibrium climate sensitivity for a doubling of atmospheric carbon dioxide (CO_2) concentrations (ECS_{2xC}) from preindustrial times has been established as a well-defined standard measure (*1*). Moreover, because transient (disequilibrium) climate change and impacts on ecological and social systems typically scale with ECS_{2xC}, it is a useful and important diagnostic in climate modeling (*1*). Initial estimates of $ECS_{2xC} = 3 \pm 1.5$ K suggested a large uncertainty (*2*), which has not been reduced in the past 32 years despite considerable efforts (*1*–*10*). On the contrary, many recent studies suggest a small possibility of very high (up to 10 K and higher) values for ECS_{2xC} (*3*–*10*), implying extreme

[1]College of Oceanic and Atmospheric Sciences, Oregon State University, Corvallis, OR 97331–5503, USA. [2]Woodrow Wilson School of Public and International Affairs, Princeton University, NJ 08544, USA. [3]Department of Earth and Planetary Sciences, Harvard University, Cambridge, MA 02138, USA. [4]Department of Earth and Atmospheric Sciences, Cornell University, Ithaca, NY 14850, USA. [5]Department of Geosciences, Oregon State University, Corvallis, OR 97331, USA. [6]Department of Geography, University of Oregon, Eugene, OR 97403, USA. [7]Institució Catalana de Recerca i Estudis Avançats and Institute of Environmental Science and Technology, Autonomous University of Barcelona, Bellaterra, Spain.

*To whom correspondence should be addressed. E-mail: aschmitt@coas.oregonstate.edu

Downloaded from www.sciencemag.org on December 12, 2011

climate changes in the near future, which would be difficult to avoid. Efforts to use observations from the past 150 years to constrain the upper end of ECS_{2xC} have met with limited success, largely because of uncertainties associated with aerosol forcing and ocean heat uptake (*8*, *9*). Data from the Last Glacial Maximum (LGM), 19,000 to 23,000 years ago, are particularly useful to estimate ECS_{2xC} because large differences from preindustrial climate and much lower atmospheric CO_2 concentrations [185 parts per million (ppm) versus 280 ppm preindustrial] provide a favorable signal-to-noise ratio, both radiative forcings and surface temperatures are relatively well constrained from extensive paleoclimate reconstructions and modeling (*11*–*13*), and climate during the LGM was close to equilibrium, avoiding uncertainties associated with transient ocean heat uptake.

Here, we combine a climate model of intermediate complexity with syntheses of temperature reconstructions from the LGM to estimate ECS_{2xC} using a Bayesian statistical approach. LGM, CO_2 doubling, and preindustrial control simulations are integrated for 2000 years using an ensemble of 47 versions of the University of Victoria (UVic) climate model (*14*) with different climate sensitivities ranging from ECS_{2xC} = 0.3 to 8.3 K considering uncertainties in water vapor, lapse rate and cloud feedback on the outgoing infrared radiation (fig. S1), as well as uncertainties in dust forcing and wind-stress response. The LGM simulations include larger continental ice sheets, lower greenhouse gas concentrations, higher atmospheric dust levels (fig. S2), and changes in the seasonal distribution of solar radiation [see supporting online material (SOM)]. We combine recent syntheses of global sea surface temperatures (SSTs) from the Multiproxy Approach for the Reconstruction of the Glacial Ocean (MARGO) project (*12*) and SATs over land, based on pollen evidence (*13*) with additional data from ice sheets and land and ocean temperatures (figs. S3 and S4; all reconstructions include error estimates). The combined data set covers over 26% of Earth's surface (Fig. 1A).

Figure 2 compares reconstructed zonally averaged surface temperatures with model results. Models with ECS_{2xC} < 1.3 K underestimate the cooling at the LGM almost everywhere, particularly at mid-latitudes and over Antarctica, whereas models with ECS_{2xC} > 4.5 K overestimate the cooling almost everywhere, particularly at low latitudes. High-sensitivity models (ECS_{2xC} > 6.3 K) show a runaway effect resulting in a completely ice-covered planet. Once snow and ice cover reach a critical latitude, the positive ice-albedo feedback is larger than the negative feedback because of reduced longwave radiation (Planck feedback), triggering an irreversible transition (fig. S5) (*15*). During the LGM, Earth was covered by more ice and snow than it is today, but continental ice sheets did not extend equatorward of ~40°N/S, and the tropics and subtropics were ice free except at high altitudes. Our model thus suggests that large climate sensitivities (ECS_{2xC} > 6 K) cannot be reconciled with paleoclimatic and geologic evidence and hence should be assigned near-zero probability.

Posterior probability density functions (PDFs) of the climate sensitivity are calculated by Bayesian inference, using the likelihood of the observations ΔT_{obs} given the model $\Delta T_{mod}(ECS_{2xC})$ at the locations of the observations. The two are assumed to be related by an error term ε; $\Delta T_{obs} = \Delta T_{mod}(ECS_{2xC}) + \varepsilon$, which represents errors in both the model (endogenously estimated separately for land and ocean; fig. S13) and the observations (fig. S3), including spatial autocorrelation. A Gaussian likelihood function and an autocorrelation length scale of λ = 2000 km are assumed. The choice of the autocorrelation length scale is motivated by the model resolution and by residual analysis. (See sections 5 and 6 in the SOM for a full description of the statistical method, assumptions, and sensitivity tests.)

The resulting PDF (Fig. 3), considering both land and ocean reconstructions, is multimodal and displays a broad maximum with a double peak between 2 and 2.6 K, smaller local maxima around 2.8 and 1.3 K, and vanishing probabilities below 1 K and above 3.2 K. The distribution has its mean and median at 2.2 and 2.3 K, respectively, and its 66 and 90% cumulative probability intervals are 1.7 to 2.6 K and 1.4 to 2.8 K, respectively. Using only ocean data, the PDF changes little, shifting toward slightly lower values (mean 2.1 K, median 2.2 K, 66% 1.5 to 2.5 K, and 90% 1.3 to 2.7 K), whereas using only land data leads to a much larger shift toward higher values (mean and median 3.4 K, 66% 2.8 to 4.1 K, and 90% 2.2 to 4.6 K).

The best-fitting model (ECS_{2xC} = 2.4 K) reproduces well the reconstructed global mean cooling of 2.2 K (within two significant digits), as well as much of the meridional pattern of the zonally averaged temperature anomalies (correlation coefficient r = 0.8) (Fig. 2). Substantial discrepancies occur over Antarctica, where the model underestimates the observed cooling by almost 4 K, and between 45° to 50° in both hemispheres, where the model is also too warm. Simulated temperature changes over Antarctica show considerable spatial variations (Fig. 1B), with larger cooling of more than 7 K over the West Antarctic Ice Sheet. The observations are located along a strong meridional gradient (fig. S7). Zonally averaged cooling of air temperatures is about 7 K at 80°S, more consistent with the reconstructions than the simulated temperature change at the locations of the observations. Underestimated ice sheet height at these locations could be a reason for the bias (*16*), as could deficiencies of the simple energy balance atmospheric model component. Underestimated cooling at mid-latitudes for the best fitting model also points to systematic model problems, such as the neglect of wind or cloud changes.

Two-dimensional features in the reconstructions are less well reproduced by the model (r = 0.5) (Fig. 1). Large-scale patterns that are qualitatively captured (Fig. 1) are stronger cooling over land than over the oceans, and more cooling at mid- to high latitudes (except for sea ice covered oceans), which is contrasted by less cooling in the central Pacific and over the Southern Hemisphere subtropical oceans. Continental cooling north of 40°N of 7.7 K predicted by the best-

Downloaded from www.sciencemag.org on December 12, 2011

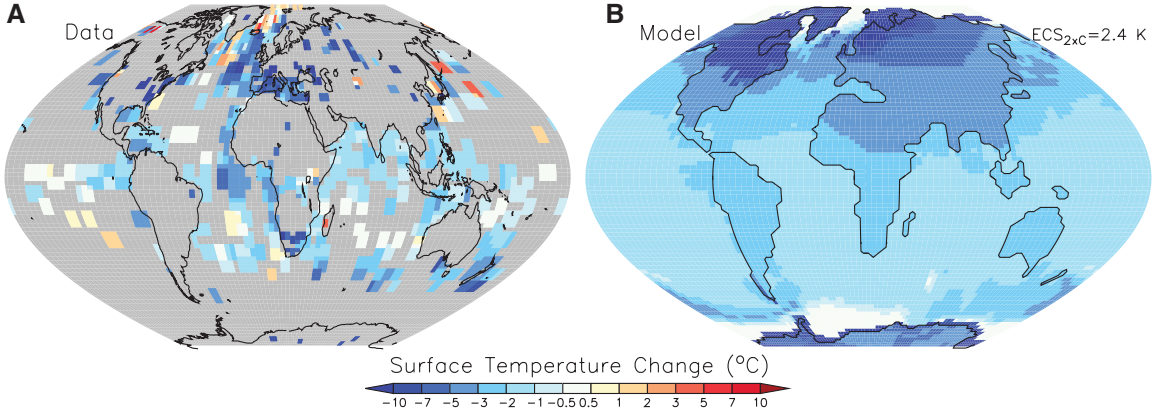

Fig. 1. Annual mean surface temperature (SST over oceans and SAT over land) change between the LGM and modern. (**A**) Reconstructions of ΔSSTs from multiple proxies (*12*), ΔSATs over land from pollen (*13*), and additional data (SOM). (**B**) Best-fitting model simulation (ECS_{2xC} = 2.4 K).

fitting model is consistent with the independent estimate of 8.3 ± 1 K from inverse ice-sheet modeling (*17*).

Generally, the model solution is much smoother than the reconstructions, partly because of the simple diffusive energy balance atmospheric model component. The model does not simulate warmer surface temperatures anywhere, whereas the reconstructions show warming in the centers of the subtropical gyres in parts of the northwest Pacific, Atlantic, and Alaska. It systematically underestimates cooling over land and overestimates cooling of the ocean (fig. S8). The land-sea contrast, which is governed by less availability of water for evaporative cooling over land compared with the ocean (*18*), is therefore underestimated, consistent with the tension between the ECS_{2xC} inferred from ocean-only versus land-only data (Fig. 3). A possible reason for this bias could be overestimated sea-to-land water vapor transport in the LGM model simulations, perhaps due to too high moisture diffusivities. Other model simplifications, such as neglecting changes in wind velocities and clouds or errors in surface albedo changes in the dynamic vegetation model component, could also contribute to the discrepancies. The ratio between low latitude (40° S to 40° N) land and sea temperature change in the best-fitting model is 1.2, which is lower than the modern ratio of 1.5 found in observations and modeling studies (*19*).

Despite these shortcomings, the best-fitting model is within the 1σ-error interval of the reconstructed temperature change in three quarters (75%, mostly over the oceans) of the global surface area covered by reconstructions (fig. S8). The model provides data-constrained estimates of global mean (including grid points not covered by data) cooling of near-surface air temperatures $\Delta SAT_{LGM} = -3.0$ K [66% probability range (–2.1, –3.3), 90% (–1.7, –3.7)] and sea surface temperatures $\Delta SST_{LGM} = -1.7$ K [66% (–1.1, –1.8), 90% (–0.9, –2.1)] during the LGM (including an increase of marine sea and air temperatures of 0.3 and 0.47 K, respectively, due to 120-m sea-level lowering; otherwise, $\Delta SAT_{LGM} = -3.3$ K and $\Delta SST_{LGM} = -2.0$ K).

The ranges of 66 and 90% cumulative probability intervals, as well as the mean and median ECS_{2xC} values, from our study are considerably lower than previous estimates. The most recent assessment report from the Intergovernmental Panel on Climate Change (*6*), for example, used a most likely value of 3.0 K and a likely range (66% probability) of 2 to 4.5 K, which was supported by other recent studies (*1*, *20*–*23*).

We propose three possible reasons that our study yields lower estimates of ECS_{2xC} than previous work that also used LGM data. First, the new reconstructions of LGM surface temperatures show less cooling than previous studies. Our best estimates for global mean (including grid points not covered by data) SAT and SST changes reported above are 30 to 40% smaller than previous estimates (*21*, *23*). This is consistent with less cooling of tropical SSTs (–1.5 K, 30°S to 30°N) in the new reconstruction (*12*) compared with previous data sets (–2.7 K) (*24*). Tropical Atlantic SSTs between 20°S and 20°N are estimated to be only 2.4 K colder during the LGM in the new reconstruction compared with 3 K used in (*23*), explaining part of the difference between their higher estimates of ECS_{2xC} and ΔSAT_{LGM} (–5.8 K).

The second reason is limited spatial data coverage. A sensitivity test excluding data from the North Atlantic leads to more than 0.5 K lower ECS_{2xC} estimates (SOM section 7 and fig. S14 and S15). This shows that systematic biases can result from ignoring data outside selected regions, as done in previous studies (*22*, *23*), and implies that global data coverage is important for estimating ECS_{2xC}. Averaging over all grid points in our model leads to a higher global mean temperature (SST over ocean, SAT over land) change (–2.6 K) than using only grid points where paleoclimate data are available (–2.2 K), suggesting that the existing data set is still spatially biased toward low latitudes and/or oceans. Increased spatial coverage of climate reconstructions is therefore necessary to improve ECS_{2xC} estimates.

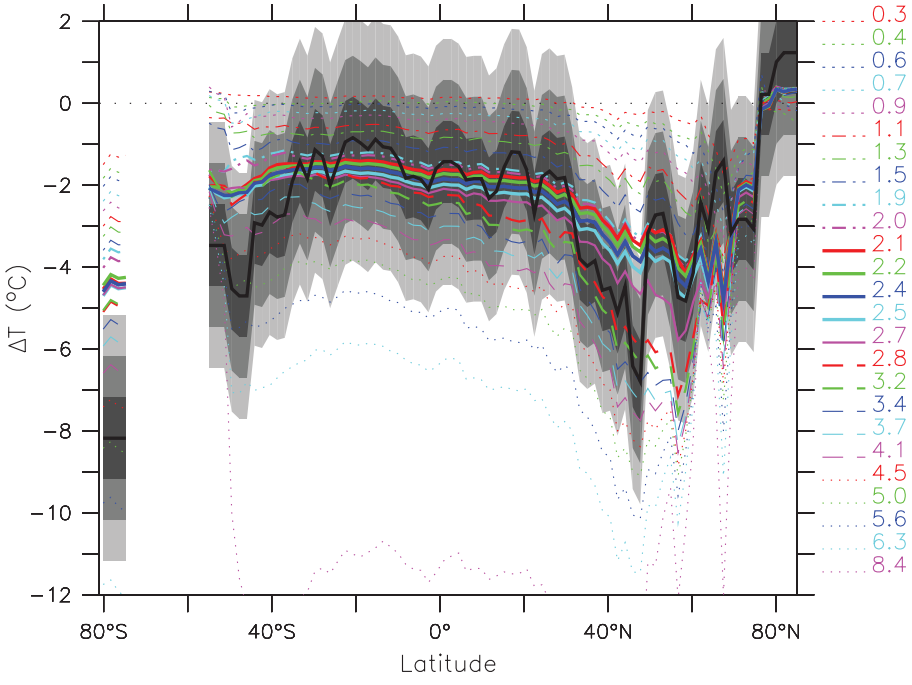

Fig. 2. Zonally averaged surface temperature change between the LGM and modern. The thick black line denotes the climate reconstructions, and the gray shading the ±1, 2, and 3 K intervals around the observations. Modeled temperatures, averaged using only cells with reconstructions (see Fig. 1), are shown as colored lines labeled with the corresponding ECS_{2xC} values.

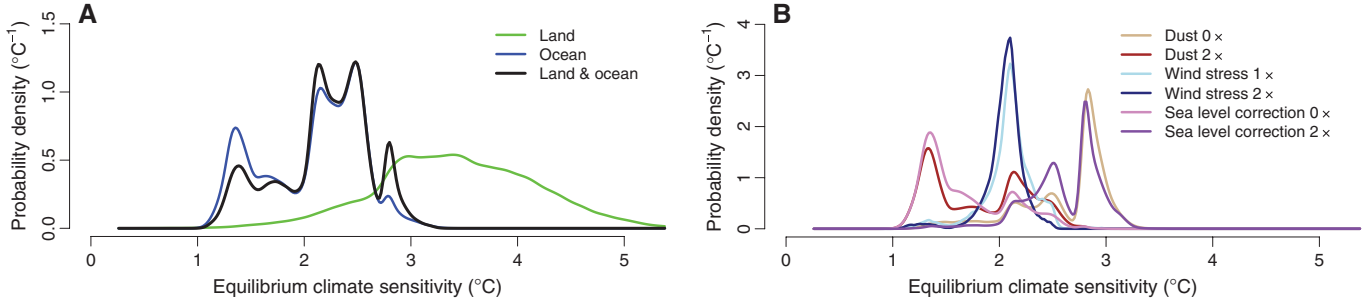

Fig. 3. Marginal posterior PDFs for ECS_{2xC}. (**A**) Estimated from land and ocean, land-only, and ocean-only temperature reconstructions using the standard assumptions (1 × dust, 0 × wind stress, 1 × sea-level correction of $\Delta SST_{SL} = 0.32$ K) (see SOM). (**B**) Estimated under alternate assumptions about dust forcing, wind stress, and ΔSST_{SL} using land and ocean data.

Downloaded from www.sciencemag.org on December 12, 2011

A third reason may be the neglect of dust radiative forcing in some previous LGM studies (*21*) despite ample evidence from the paleoenvironmental record that dust levels were much higher (*25*, *26*). Sensitivity tests (Fig. 3) (SOM section 7) show that dust forcing decreases the median ECS_{2xC} by about 0.3 K.

Our estimated ECS_{2xC} uncertainty interval is rather narrow, <1.5 K for the 90% probability range, with most (~75%) of the probability mass between 2 and 3 K, which arises mostly from the SST constraint. This sharpness may imply that LGM SSTs are a strong physical constraint on ECS_{2xC}. However, it could also be attributable to overconfidence arising from physical uncertainties not considered here, or from misspecification of the statistical model.

To explore this, we conduct sensitivity experiments that perturb various physical and statistical assumptions (Fig. 3 and figs. S14 and S15). The experiments collectively favor sensitivities between 1 and 3 K. However, we cannot exclude the possibility that the analysis is sensitive to uncertainties or statistical assumptions not considered here, and the underestimated land/sea contrast in the model, which leads to the difference between land- and ocean-based estimates of ECS_{2xC}, remains an important caveat.

Our uncertainty analysis is not complete and does not explicitly consider uncertainties in radiative forcing due to ice-sheet extent or different vegetation distributions. Our limited model ensemble does not scan the full parameter range, neglecting, for example, possible variations in shortwave radiation due to clouds. Nonlinear cloud feedback in different complex models make the relation between LGM and CO_2 doubling–derived climate sensitivity more ambiguous than apparent in our simplified model ensemble (*27*). More work, in which these and other uncertainties are considered, will be required for a more complete assessment.

In summary, using a spatially extensive network of paleoclimate observations in combination with a climate model, we find that climate sensitivities larger than 6 K are implausible, and that both the most likely value and the uncertainty range are smaller than previously thought. This demonstrates that paleoclimate data provide efficient constraints to reduce the uncertainty of future climate projections.

References and Notes

1. R. Knutti, G. C. Hegerl, *Nat. Geosci.* **1**, 735 (2008).
2. J. G. Charney *et al.*, *Carbon Dioxide and Climate: A Scientific Assessment* (National Academy of Sciences, Washington, DC, 1979).
3. D. A. Stainforth *et al.*, *Nature* **433**, 403 (2005).
4. G. H. Roe, M. B. Baker, *Science* **318**, 629 (2007).
5. D. L. Royer, R. A. Berner, J. Park, *Nature* **446**, 530 (2007).
6. IPCC, *Climate Change 2007: The Physical Science Basis. Contribution of Working Group I to the Fourth Assessment Report of the Intergovernmental Panel on Climate Change*. S. Solomon *et al.*, Eds. (Cambridge University Press, Cambridge, 2007), pp. 996.
7. R. Knutti, T. F. Stocker, F. Joos, G. K. Plattner, *Clim. Dyn.* **21**, 257 (2003).
8. C. E. Forest, P. H. Stone, A. P. Sokolov, *Tellus, Ser. A, Dyn. Meterol. Oceanogr.* **60**, 911 (2008).
9. N. G. Andronova, M. E. Schlesinger, *J. Geophys. Res. Atmos.* **106**, (D19), 22605 (2001).
10. J. M. Gregory, R. J. Stouffer, S. C. B. Raper, P. A. Stott, N. A. Rayner, *J. Clim.* **15**, 3117 (2002).
11. N. M. Mahowald *et al.*, *J. Geophys. Res. Atmos.* **111**, (D10), D10202 (2006).
12. MARGO Project Members, *Nat. Geosci.* **2**, 127 (2009).
13. P. Bartlein *et al.*, *Clim. Dyn.* **37**, 775 (2011).
14. A. J. Weaver *et al.*, *Atmos.-ocean* **39**, 361 (2001).
15. M. I. Budyko, *Tellus* **21**, 611 (1969).
16. V. Masson-Delmotte *et al.*, *Clim. Dyn.* **26**, 513 (2006).
17. R. Bintanja, R. S. W. van de Wal, J. Oerlemans, *Clim. Dyn.* **24**, 197 (2005).
18. S. Manabe, M. J. Spelman, R. J. Stouffer, *J. Clim.* **5**, 105 (1992).
19. R. T. Sutton, B. W. Dong, J. M. Gregory, *Geophys. Res. Lett.* **34**, L02701 (2007).
20. J. D. Annan, J. C. Hargreaves, *Geophys. Res. Lett.* **33**, L06704 (2006).
21. J. Hansen *et al.*, *The Open Atmospheric Science Journal* **2**, 217 (2008).
22. D. W. Lea, *J. Clim.* **17**, 2170 (2004).
23. T. Schneider von Deimling, H. Held, A. Ganopolski, S. Rahmstorf, *Clim. Dyn.* **27**, 149 (2006).
24. A. P. Ballantyne, M. Lavine, T. J. Crowley, J. Liu, P. B. Baker, *Geophys. Res. Lett.* **32**, L05712 (2005).
25. S. P. Harrison, K. E. Kohfeld, C. Roelandt, T. Claquin, *Earth Sci. Rev.* **54**, 43 (2001).
26. B. A. Maher *et al.*, *Earth Sci. Rev.* **99**, 61 (2010).
27. M. Crucifix, *Geophys. Res. Lett.* **33**, L18701 (2006).

Acknowledgments: This work was supported by the Paleoclimate Program of the National Science Foundation through project PALEOVAR (06023950-ATM). Thanks to S. Harrison and two anonymous reviewers for thoughtful and constructive comments that led to substantial improvements in the paper.

Supporting Online Material

www.sciencemag.org/cgi/content/full/science.1203513/DC1
Materials and Methods
SOM Text
Figs. S1 to S16
Table S1
References (*28*–*103*)

28 January 2011; accepted 20 October 2011
Published online 24 November 2011;
10.1126/science.1203513

Middle Stone Age Bedding Construction and Settlement Patterns at Sibudu, South Africa

Lyn Wadley,[1,2]* Christine Sievers,[1] Marion Bamford,[3] Paul Goldberg,[4,5] Francesco Berna,[5] Christopher Miller[4]

The Middle Stone Age (MSA) is associated with early behavioral innovations, expansions of modern humans within and out of Africa, and occasional population bottlenecks. Several innovations in the MSA are seen in an archaeological sequence in the rock shelter Sibudu (South Africa). At ~77,000 years ago, people constructed plant bedding from sedges and other monocotyledons topped with aromatic leaves containing insecticidal and larvicidal chemicals. Beginning at ~73,000 years ago, bedding was burned, presumably for site maintenance. By ~58,000 years ago, bedding construction, burning, and other forms of site use and maintenance intensified, suggesting that settlement strategies changed. Behavioral differences between ~77,000 and 58,000 years ago may coincide with population fluctuations in Africa.

Genetic and phenotypic (skull) data indicate that after 80 thousand years ago (ka), human populations went through bottlenecks, isolations, and subsequent expansions (*1*–*3*). Concurrently, the Middle Stone Age (MSA) of South Africa witnessed a variety of emerging behavioral practices by anatomically modern humans, including use of shell beads and engraving (*4*–*6*), innovative stone technology (*7*), the creation and use of compound adhesives (*8*), heat-treatment of rock (*9*), and circumstantial evidence for snares (*10*) and bows and arrows (*11*). Less emphasis has been placed on innovations in domestic organization and settlement strategies, which might also have been influenced by major demographic changes that were occurring in Africa. Here, we present geoarchaeological and archaeobotanical evidence (*12*) from the South African rock shelter Sibudu (fig. S1) for changing domestic practices in the form of construction of plant bedding starting at ~77 ka, approximately 50,000 years earlier than records elsewhere. Most evidence for bedding in the Pleistocene has been inferential, except for that from Esquilleu Cave, Spain (*13*); Strathalan B Cave, South Africa, dated 29 to 26 ka (*14*); and Ohalo II, Israel, dated to 23 ka (*15*).

Sibudu is situated on a cliff 20 m above the uThongathi River (figs. S2 and S3), 40 km north of Durban and 15 km inland from the Indian Ocean. Excavations have been conducted here

[1]School of Geography, Archaeology, and Environmental Studies, University of the Witwatersrand, Johannesburg 2050, South Africa. [2]Institute for Human Evolution, University of the Witwatersrand, Johannesburg 2050, South Africa. [3]Bernard Price Institute for Palaeontological Research, University of the Witwatersrand, Johannesburg 2050, South Africa. [4]Institute for Archaeological Sciences, Universität Tübingen, Tübingen 72070, Germany, [5]Department of Archaeology, Boston University, Boston, MA 02215, USA.

*To whom correspondence should be addressed. E-mail: lyn.wadley@wits.ac.za

Downloaded from www.sciencemag.org on December 12, 2011